ACS OMEGA

Article

Cite This: ACS Omega 2019, 4, 5661−5669

http://pubs.acs.org/journal/acsodf

Quasiparticle *GW* Calculations on Lead-Free Hybrid Germanium Iodide Perovskite $CH_3NH_3GeI_3$ for Photovoltaic Applications

Deivasigamani Umadevi* and Graeme W. Watson*

School of Chemistry and CRANN, Trinity College Dublin, The University of Dublin, Dublin D2, Ireland

Supporting Information

ABSTRACT: Lead-free organic−inorganic halide perovskites have gained much attention as nontoxic alternatives to $CH_3NH_3PbI_3$ in next-generation solar cells. In this study, we have examined the geometric and electronic properties of methylammonium germanium iodide $CH_3NH_3GeI_3$ using density functional theory. Identifying a suitable functional to accurately model the germanium halide perovskites is crucial to allow the theoretical investigation for tuning the optoelectronic properties. The performance of various functionals (PBE, PBE+D3, PBEsol, PBEsol+D3, HSE06, and HSE06+D3) has been evaluated for modelling the structure and properties. The calculation of electronic properties was further refined by using the quasiparticle *GW* method on the optimized geometries, and that has an excellent agreement with the experiment. We report from our *GW* calculations that the characteristic of the density of states for $CH_3NH_3GeI_3$ resembles the density of states for $CH_3NH_3PbI_3$ and the effective masses of the charge carriers of $CH_3NH_3GeI_3$ are comparable to the effective masses of $CH_3NH_3PbI_3$ as well as silicon used in commercially available solar cells.

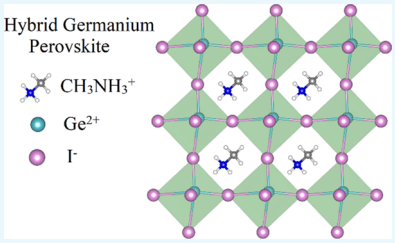

INTRODUCTION

Efficient and cost-effective harvesting of solar energy is a major challenge in photovoltaics, which can meet the demands in future energy challenges.[1] Though crystalline silicon photovoltaics dominate the solar-cell market presently, there are still a lot of issues related to high manufacturing cost and recombinational, reflection, and absorption losses along with efficiency issues.[2,3] Lead-based hybrid organic−inorganic halide perovskite ($CH_3NH_3PbI_3$) represents a major breakthrough in the field of low-cost photovoltaic materials.[4,5] Kojima et al. explored $CH_3NH_3PbI_3$ as a light harvester in liquid-based dye-sensitized solar cells for the first time in 2009.[6] Since then, the power conversion efficiencies of lead hybrid perovskites have increased from 3.8 to over 23.7% within a decade.[6−8] The significant performance of the hybrid perovskites can be attributed to their appropriate band gaps, large carrier lifetimes, and long carrier diffusion lengths.[9,10] Solar cells based on hybrid perovskite $CH_3NH_3PbI_3$ have therefore become a prospective alternative to conventional photovoltaics owing to their efficiency, low cost and simple processing.[11] Theoretical studies have been key to understanding the properties that encompass the structure, stability, bandgaps, band alignments, and dielectric properties of hybrid perovskites.[12−18] Walsh and co-workers have made significant contributions in understanding the photovoltaic performance of hybrid perovskites through their theoretical studies that includes the effects of ferroelectric tendencies,[19−22] cation dynamics,[23] polyanion substitution,[24] halogen replacement,[25] defects,[26,27] band gap engineering,[28] phonon anharmonicity,[29] and other physical properties.[30] De Angelis and co-workers have brought added insights into the structure, properties, and factors that influence the exciton binding energy through their theoretical studies.[31−36] Motta et al. studied the role of organic cations in $CH_3NH_3PbI_3$ and revealed that molecular rotations of the organic cation with the resulting dynamical change in the band structure might be the origin of the slow carrier recombination and the greater conversion efficiency of $CH_3NH_3PbI_3$.[37]

Despite the huge potential of the hybrid perovskite $CH_3NH_3PbI_3$, there are two main drawbacks: the instability of the materials, which decompose in the presence of humid air,[38] and the toxicity of lead. Modifications in the organic structures such as long alkyl chains and layered structures have been suggested as mechanisms to increase the stability of lead halide perovskites.[39,40] To improve the stability without affecting the performance, methylammonium has been partially replaced by cesium in lead halide solar cell devices.[41,42] Scanlon and co-workers explored the efficacy of various solar absorbers beyond $CH_3NH_3PbI_3$,[43−46] cation replacement structures[47,48] and anion replacement structures,[49,50] to obtain stable and efficient photovoltaic materials. However, it has become increasingly important to replace lead to develop nontoxic and eco-friendly alternative light-harvesting hybrid materials. The Sn-based perovskite $CH_3NH_3SnI_3$ has been shown to have a similar structure to $CH_3NH_3PbI_3$, but studies show that it suffers from low efficiency.[51−54] Moving from perovskite to double perovskite such as $Cs_2AgBiBr_6$ is considered as an approach where lead can be replaced by nontoxic cations.[44,55,56] Zhao et al. employed a cation-transmutation method to design lead-free inorganic halide

Received: November 26, 2018
Accepted: March 8, 2019
Published: March 21, 2019

DOI: 10.1021/acsomega.8b03291
ACS Omega 2019, 4, 5661−5669

perovskites such as $Cs_2InSbCl_6$ and $Cs_2InBiCl_6$, although In is already overused in transparent conducting oxides (TCOs).[57]

Germanium-based materials have recently received attention as potential candidates for nontoxic photovoltaics as germanium belongs to the same group as lead and tin.[58−60] Kanatzidis and co-workers synthesized a broad and structurally diverse family of polar hybrid perovskites based on the trigonal pyramidal $[GeI_3]^-$ building block.[61] Krishnamoorthy et al. synthesized germanium-based hybrid perovskite materials and reported the power conversion efficiency of $CsGeI_3$ to be 0.11% and $CH_3NH_3GeI_3$ to be 0.20%.[62] Germanium-based hybrid perovskites are also expected to have drawbacks such as instability due to oxidation from (II) to (IV) as also observed in the case of tin(II)-based perovskites. In general, the relative stability of the 2+ oxidation state increases from carbon to lead (Ge^{2+} < Sn^{2+} < Pb^{2+}). Nevertheless, their stability in a confined environment may depend on various factors such as the size of the cations. Sun et al. compared the stability of Pb-, Sn-, and Ge- based hybrid perovskites using density functional theory and found that the order of stability is $CH_3NH_3PbI_3$ > $CH_3NH_3GeI_3$ > $CH_3NH_3SnI_3$.[63] However, so far, to the best of our knowledge, there is no experimental evidence to compare the stability of $CH_3NH_3GeI_3$ and $CH_3NH_3SnI_3$. Zhao et al. reported that applying compressive strain on $CH_3NH_3GeI_3$ enables it to achieve superior optical absorption and transport properties.[64] The reported theoretical band gaps for $CH_3NH_3GeI_3$ exhibit significant discrepancies: the band gaps obtained using the PBE method ranges from 1.17 to 1.61 eV[58,59,63] and those of the hybrid functional range from 1.70 to 2.04 eV.[58,63] Hence, it is vital to identify an accurate computational method for further investigation on tuning the structure and properties of $CH_3NH_3GeI_3$.

In this article, a systematic structural evaluation of $CH_3NH_3GeI_3$ has been performed employing different DFT and hybrid DFT methods to analyze the accuracy of each method to reproduce the experimental structure and electronic structure. The band structure, band gap, optical absorption, and effective masses of $CH_3NH_3GeI_3$ have been investigated in detail. Total and partial electronic density-of-states analyses of $CH_3NH_3GeI_3$ are used to understand the electronic contributions to the band edges. We resolve the ambiguity of the band gap by performing the first state-of-the-art many-body perturbation theory calculations in the *GW* approximation on $CH_3NH_3GeI_3$. The electronic properties of $CH_3NH_3GeI_3$ obtained from this study are compared with those of $CH_3NH_3PbI_3$ from the literature in order to evaluate the ability of $CH_3NH_3GeI_3$ as a nontoxic replacement.

RESULTS AND DISCUSSION

$CH_3NH_3GeI_3$ rhombohedral perovskite unit cells (12 atoms per cell) were optimized starting from the trigonal structure with the *R*3*m* space group as determined by X-ray diffraction at 293 K.[61] The 12-atom unit cell used in this structure may not be able to capture the possible octahedral tilts and symmetry breaking in the dynamic structure.[65,66] Hybrid perovskite often displays a dynamic average structure at room temperature, and results from average structures have been often shown to give good insight into the electronic properties.[60,67] The unit cell consists of corner-linked distorted octahedra of the I anions, with the Ge cation at their center and the CH_3NH_3 cation between them (Figure 1). There are two types of Ge−I bonds in the GeI_6 octahedra in which Ge−I(1) is shorter than Ge−I(2). The lattice parameters of the optimized structures of

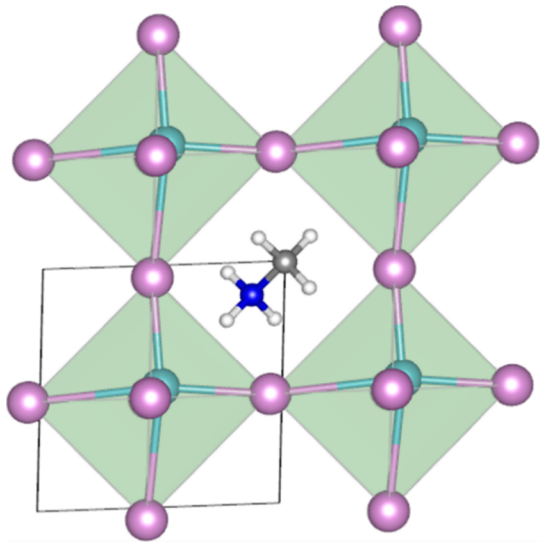

Figure 1. Optimized structure of the $CH_3NH_3GeI_3$ rhombohedral perovskite unit cells. The color codes are considered as follows: green, Ge; purple, I; grey, C; blue, N; and white, H.

$CH_3NH_3GeI_3$ such as lattice vector (a), angle (α), volume (V), and the bond distances of Ge−I(1), Ge−I(2), and C−N are given in Table 1. Calculation carried out using PBEsol displays an underestimation of the lattice vector, angle, volume, and Ge−I(2) bond distance. It predicts that the angle and Ge−I(1) bond distance are similar to the experimental values. PBE overestimates the lattice vectors, volume, and Ge−I(2) bond length. The angle (0.62% error) and the Ge−I(1) bond distance (0.25% error) calculated from PBE are in good agreement with the experimental values. HSE06 overestimates the lattice vector, volume, and Ge−I(2) bond distance and underestimates the angle and Ge−I(1) bond distance. The inclusion of dispersion corrections causes a reduction in the unit cell volume and associated bond lengths. PBEsol+D3 significantly underestimates all the lattice parameters and bond lengths. The parameters predicted from PBE+D3 are in good agreement with the experimental structural parameters of $CH_3NH_3GeI_3$ with the lattice vector reproduced within 0.94%, angle by 1.30%, volume by 3.11%, Ge−I(1) by 0.11%, and Ge−I(2) by 1.36%. HSE06+D3 calculations are in good agreement with the experimental lattice vector, volume, and Ge−I(2) bond distance. They underestimate the angle and Ge−I(1) bond distance. Our calculated C−N bond lengths by all the methods considered are higher than the experimental value. The difference may be due to the finite temperature measurement (293 K) of the experiment. Reviewing the literature on C−N bond lengths in hybrid perovskites shows an interesting variation. At low temperature, the bond length matches that expected from the benchmark ammonium ion[68] and agrees with computational work (see Table S1).[69−71] The bond length also agrees well with low-temperature (<200 K) experimental structural data.[72−74] At higher temperatures (>290 K), the bond lengths appear to shrink below 1.4 Å, which is more than likely an artifact of the dynamical motion of the cation.[75,76]

The band structures calculated along high symmetry directions in the Brillouin zone using PBE+D3 are given in Figure 2a. All of the methods used give rise to similar band structures except with different band gaps (see Supporting Information, Figure S1). $CH_3NH_3GeI_3$ is characterized by a

DOI: 10.1021/acsomega.8b03291
ACS Omega 2019, 4, 5661−5669

Table 1. Lattice Parameters and Structural Parameters of $CH_3NH_3GeI_3$ by Employing Various DFT and Hybrid DFT Methods[a]

parameter	experiment	PBEsol	PBE	HSE06	PBEsol+D3	PBE+D3	HSE06+D3
a (Å)	6.183	6.014 (−2.73)	6.298 (1.86)	6.273 (1.46)	5.907 (−4.46)	6.125 (−0.94)	6.102 (−1.31)
α (°)	87.527	86.658 (−0.99)	86.988 (−0.62)	86.284 (−1.42)	86.420 (−1.26)	86.390 (−1.30)	85.795 (−1.97)
V (Å^3)	235.74	216.41 (−8.20)	248.80 (5.54)	245.35 (4.08)	204.96 (−13.06)	228.42 (−3.11)	225.50 (−4.34)
Ge−I(1) (Å)	2.772	2.775 (0.11)	2.779 (0.25)	2.733 (−1.41)	2.769 (−0.11)	2.775 (0.11)	2.728 (−1.59)
Ge−I(2) (Å)	3.446	3.276 (−4.93)	3.564 (3.42)	3.587 (4.09)	3.171 (−7.98)	3.399 (−1.36)	3.428 (−0.52)
C−N (Å)	1.370	1.479 (7.95)	1.493 (8.98)	1.482 (8.17)	1.476 (7.30)	1.492 (8.91)	1.480 (8.03)

[a]Experimental data is from ref 61, and percentages of deviation from experiments are given in parentheses.

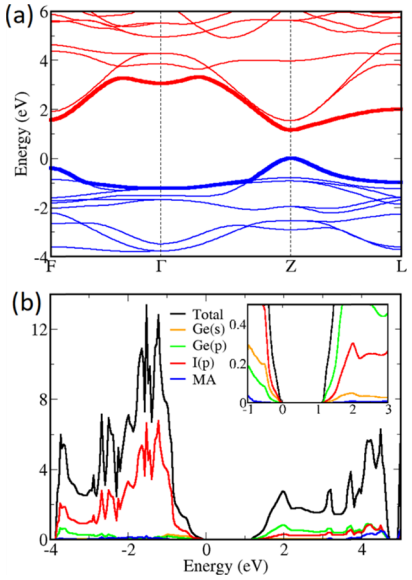

Figure 2. (a) Band structure of $CH_3NH_3GeI_3$ obtained by the PBE+D3 method. (b) Total and partial electronic densities of states of $CH_3NH_3GeI_3$ obtained by the PBE+D3 method. The insets are enlargements of the valence band maximum (VBM) and conduction band minimum (CBM). The valence band maximum (VBM) has been set to 0 eV.

direct band gap at the Z point of the Brillouin zone for all the methods considered, indicating possible strong optical absorption. The band gaps (Table 2) for PBEsol (0.89 eV) and PBE (1.39 eV) are greatly underestimated compared to the experimental value (1.90 eV),[61] and the addition of dispersion correction further reduces these band gaps. These results are as expected as the GGA method generally underestimates the band gap of semiconductors. HSE06 predicted a band gap that is closer to the experimental result; however, the inclusion of dispersion interactions also decreases the band gap to 1.60 eV. Our calculation reveals that DFT functionals with the standard proportion of D3 dispersion identified by Grimme clearly overbind the structure.[77]

Table 2. Band Gap, Effective Mass of the Charge Carriers in the Z−Γ Direction, Reduced Mass, and Optical Band Gap of $CH_3NH_3GeI_3$ with Different Functionals

method	band gap (E_g in eV)	holes (m_h^* in m_0)	electrons (m_e^* in m_0)	reduced mass (μ in m_0)	optical gap (E_g in eV)
experiment[a]	1.90				
PBEsol	0.89	0.094	0.092	0.046	0.89
PBE	1.39	0.198	0.180	0.094	1.39
HSE06	1.95	0.195	0.160	0.088	1.95
PBEsol+D3	0.73	0.070	0.069	0.035	0.73
PBE+D3	1.15	0.137	0.131	0.067	1.15
HSE06+D3	1.60	0.145	0.142	0.072	1.60

[a]Experimental data is from ref 61.

We evaluated the effective mass (m^*) of the charge carriers at the valence band maximum (VBM) and the conduction band minimum (CBM) using the parabolic approximation. In general, highly dispersed bands signify a high degree of charge carrier delocalization, which results in high mobility and thus high conductivity. The theoretically calculated effective masses of $CH_3NH_3PbI_3$ at the PBE+D3 level are $m_h^* = 0.29$ and $m_e^* = 0.23$[67] and the reduced mass $\mu = 0.13$ ($\mu = m_e^* \cdot m_h^*/(m_e^* + m_h^*)$), while the experimentally determined reduced mass of $CH_3NH_3PbI_3$ is $0.09-0.15m_0$.[78] In Table 2, we have listed our theoretical effective masses of the holes (m_h^*) and electrons (m_e^*) and the reduced mass μ of $CH_3NH_3GeI_3$ in the Z−Γ direction for different methods. There is no significant trend observed in the effective masses obtained from different functionals. The inclusion of dispersion interaction reduces the effective masses for all the methods considered. The calculated effective masses of $CH_3NH_3GeI_3$ obtained at the PBE+D3 are smaller than those of $CH_3NH_3PbI_3$ obtained using the same method[67] and indicate excellent mobility.

We have computed the optical absorption spectrum of $CH_3NH_3GeI_3$ within the transversal approximation and PAW method.[79] The optical band gaps for all the DFT and hybrid DFT methods considered are identical to the fundamental band gaps obtained for the respective methods, indicating strong symmetry-allowed VBM-to-CBM transitions.

Figure 2b shows the total and partial densities of states of $CH_3NH_3GeI_3$. The overall shape and characteristics are found to be similar for all the other methods considered (see Figure S2 of the Supporting Information). The VBM is mainly composed of the I(p) mixed with a small percentage of Ge(s), while the CBM is mainly Ge(p) with a small contribution from I(p). As shown in the inset figure, the organic cation $CH_3NH_3^+$ has no significant contribution to the band edges. The band edge characters observed here for $CH_3NH_3GeI_3$ are consistent with the band edge characters of $CH_3NH_3PbI_3$, where the VBM is formed through Pb(s)/I(p) combination, while the CBM is formed mainly by Pb(p) orbitals.[19]

In summary, without dispersion correction, PBEsol underestimates the geometry, while PBE and HSE06 overestimate it. PBE+D3 gives rise to the best prediction of lattice parameters and the geometry. HSE06+D3 predicted the structural parameters in good agreement with the experiment, while PBEsol+D3 gave a poor reproduction of the observed structure. Qualitatively, for all the methods considered, the overall shapes of the electronic structure in terms of both the band structure and characteristics of the density of states are

DOI: 10.1021/acsomega.8b03291
ACS Omega 2019, 4, 5661−5669

found to be similar with the exception of the band gap magnitude. DFT methods largely underestimate the experimental band gap. Although HSE06 predicted a band gap that is closer to the experimental result, the addition of dispersion interactions decreases the band gap, and hence, all methods predict band gaps that are significantly smaller than the experimental values. The introduction of dispersion correction decreases the volume of the system for all functionals (Table 1). This decrease in the volume changes the overlap and thus causes a widening of the gap between the VBM and CBM. This leads to a small increase in the band dispersion and hence a decrease in the effective masses and subsequent narrowing of the band gap (Table 2). To address the electronic structure, we have performed state-of-the-art many-body perturbation theory calculations in the *GW* approximation using PBE+D3 and HSE06+D3 optimized structures. In modeling lead hybrid perovskites, it has been found that for a precise description of the electronic structure, it is required to calculate many-body quasiparticle energies, for example, in the framework of the *GW* approximation.[80−84]

Many-body perturbation theory, which is within the single-shot G_0W_0, partially self-consistent GW_0, and the self-consistent *GW* have been applied to our PBE+D3 and HSE06+D3 calculations. The band structure and electronic density of states of $CH_3NH_3GeI_3$ obtained at G_0W_0 (PBE+D3) are shown in Figure 3. Overall characteristics of the band

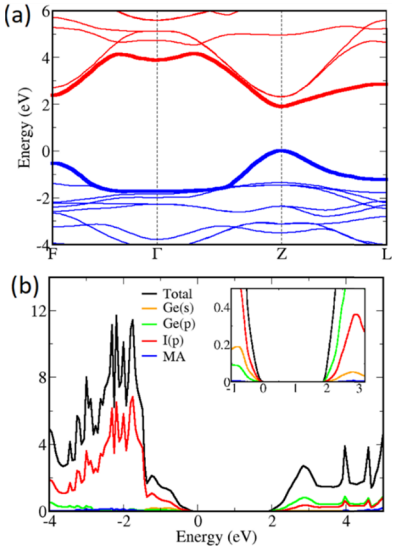

Figure 3. (a) Band structure of $CH_3NH_3GeI_3$ obtained by the G_0W_0 (PBE+D3) method. (b) Total and partial electronic densities of states of $CH_3NH_3GeI_3$ obtained by the G_0W_0 (PBE+D3) method. The insets are enlargements of the VBM and CBM. The VBM has been set to 0 eV.

structure and the density of states are found to be similar for all the *GW* methods considered (Figures S3 and S4 of the Supporting Information). The characteristics of the band structure and the density of states obtained from the *GW* calculations are in good agreement with the DFT and hybrid DFT calculations with the exception of the varying band gaps (Table 3), and hence, we are not repeating the discussion here. Our calculated band gap for G_0W_0 (PBE+D3) is in good agreement with the optical band gap reported from the experimental optical absorption, measured in diffuse reflectance mode (1.90 eV).[61] The G_0W_0 calculation on the

Table 3. Band Gap, Effective Mass, Reduced Mass of the Charge Carriers in the Z−Γ Direction, and Optical Band Gap of $CH_3NH_3GeI_3$ with *GW* Approximation

method	band gap (E_g in eV)	holes (m_h^* in m_0)	electrons (m_e^* in m_0)	reduced mass (μ in m_0)	optical gap (E_g in eV)
experiment[a]	1.90				
G_0W_0 (PBE+D3)	1.90	0.145	0.122	0.066	1.90
GW_0 (PBE+D3)	2.19	0.147	0.138	0.071	2.19
GW (PBE+D3)	2.24	0.158	0.120	0.068	2.24
G_0W_0 (HSE06+D3)	2.22	0.157	0.142	0.075	2.23
GW_0 (HSE06+D3)	2.31	0.167	0.134	0.074	2.31
GW (HSE06+D3)	2.42	0.157	0.144	0.075	2.43

[a]Experimental data is from ref 61.

HSE06+D3 geometry slightly overestimates the experimental band gap. The partially self-consistent GW_0 and the self-consistent *GW* approaches also overestimate the band gap.

The *GW* results appear confusing as what was expected to be the poorest approach (G_0W_0/PBE+D3) gave the closest agreement with the experiment. However, the impact of thermal effects on the electronic structures can be significant. Wiktor et al. considered cubic $CsPbX_3$ and $CsSnX_3$ and observed large band gap renormalization due to finite temperature.[85] They concluded that the effect of temperature will be expected to be smaller for non-cubic phases and for perovskites containing organic molecules, in which some disorder is already present at 0 K.[85] Since $CH_3NH_3GeI_3$ has a noncubic symmetry and contains organic cations, we would expect that this effect is small but may be a factor in the apparently poorer self-consistent *GW* results. In addition, the quality of G_0W_0 is known to be very dependent on the starting electronic structure.[86] This may explain why the poorer PBE+D3 electronic structure gives rise to apparently better results due to the fortuitous cancellation of errors with the thermal effect in G_0W_0/PBE+D3. Self-consistent *GW* has been found to significantly improve the situation where the starting electronic structure is poor, which is illustrated by *GW*/PBE+D3 giving a similar band gap to that obtained using G_0W_0/HSE06+D3. Self-consistent *GW* has been found to overestimate gaps,[86] which is consistent with the increase observed for G_0W_0/HSE06+D3. Here, the excellent starting point gives rise to the more advanced *GW* techniques, giving band gaps in poorer agreement with experiments than G_0W_0. van Schilfgaarde has suggested that self-consistent *GW* suffers from the inclusion of unphysical contributions, giving rise to an unreasonable *W* even for the electron gas[87,88] that may lead to this overestimation.[89]

The effective masses of electrons are slightly lower than those of holes (Table 3), which suggest that the electron mobility of this material may be better than the hole mobility as observed earlier in $CH_3NH_3PbI_3$.[67] The effective masses of $CH_3NH_3GeI_3$ calculated using G_0W_0 (PBE+D3) ($m_h^* = 0.145m_0$, $m_e^* = 0.122m_0$) are comparable with those of $CH_3NH_3PbI_3$ ($m_h^* = 0.180m_0$, $m_e^* = 0.163m_0$).[83] The effective mass of electrons (m_e^*) in silicon is estimated to be 0. $19m_0$, and the effective masses of heavy and light holes (m_h^*) are $0.54m_0$ and $0.15m_0$, respectively.[90] Hence, the effective masses of $CH_3NH_3GeI_3$ calculated by our highly reliable *GW*

DOI: 10.1021/acsomega.8b03291
ACS Omega 2019, 4, 5661−5669

calculations are comparable to those of silicon used in commercially existing solar cells, indicating potential for $CH_3NH_3GeI_3$ to be used in solar cells. The optical band gaps are in excellent agreement with the fundamental band gaps showing strong symmetry-allowed transitions.

$CH_3NH_3GeI_3$ exhibits a direct band gap, indicating strong absorption as observed in the case of $CH_3NH_3PbI_3$, and the characteristics of their density of states are also similar. In $CH_3NH_3PbI_3$, the top of the VB and the bottom of the CB are predominantly of I(p) and Pb(p) characters, respectively, which is in accordance with our observed results for $CH_3NH_3GeI_3$ where the top of the VB is predominantly I(p) and the bottom of the CB is predominantly of Ge(p) states. Nevertheless, $CH_3NH_3GeI_3$ exhibits a band gap of 1.90 eV, which is higher than that of the widely studied $CH_3NH_3PbI_3$ (1.50 eV). According to the Shockley−Queisser limit, an ideal solar cell absorber material is considered to be a semiconductor with a direct optical band gap of approximately 1.50 eV.[91] $CH_3NH_3GeI_3$ with its larger band gap may be suitable for photovoltaic applications as a top layer in a tandem solar cell that moderates the efficiency losses by using multisemiconductor layers with different band gaps. Replacement studies on $CH_3NH_3GeI_3$ by various organic cations, halides, mixed halides, mixed metals, and mixed organic cations could be useful for tuning the structural, electrical, and optoelectronic properties. The capability of the *GW* calculations to reproduce the experimental results indicates that this procedure could be used to predict the band gaps of germanium-based hybrid halide perovskites, which show potential for applications in solar cells. The systematic assessment of the performance of various functionals in this work is expected to provide valuable guidance in further theoretical investigations for tuning the optoelectronic properties of $CH_3NH_3GeI_3$.

CONCLUSIONS

The structure, electronic properties, and optical properties of $CH_3NH_3GeI_3$ were systematically investigated using a range of theoretical methods. We have demonstrated that the combination of PBE+D3 geometry and G_0W_0 calculations exhibits better agreement with experimental values, in regard to both geometric and electronic structure. The fundamental band gap of the $CH_3NH_3GeI_3$ is direct in nature, and the density-of-states analysis indicates that the valence band is predominantly made up of I(p) states, while the conduction band consists primarily of Ge(p) states. The estimated effective masses from our *GW* calculations are comparable with those of $CH_3NH_3PbI_3$ as well as those of silicon used in commercial photovoltaic cells. The optical band gaps obtained are identical to the fundamental band gaps, indicating strong symmetry-allowed VBM-to-CBM transition. The characteristics of the density of states and the effective masses of the charge carriers of $CH_3NH_3GeI_3$ are in agreement with those of $CH_3NH_3PbI_3$. The band gap (1.90 eV) of $CH_3NH_3GeI_3$ indicates that it may be suitable for photovoltaic applications as a top layer in a tandem solar cell. Ultimately, we believe that this work provides a promising platform for unleashing the full potential of germanium-based perovskites for photovoltaic applications in the future.

COMPUTATIONAL METHODS

All calculations were performed within periodic boundary conditions through the Vienna ab initio simulation package (VASP),[92,93] which employs the projector-augmented wave (PAW) method[94,95] to describe interactions between the core and valence electrons. We have calculated the convergence with respect to the *k* point and plane wave cutoff and found that an 8 × 8 × 8 *k* point mesh and a 500 eV cutoff converge the energy to within 0.001 eV per atom. Calculations were performed by using different approaches toward treating the exchange and correlation to investigate their suitability in describing the structural and electronic properties. We performed calculations using the generalized gradient approximation (GGA) in the form of Perdew−Burke−Ernzerhof (PBE)[96] and PBEsol, the revised version of PBE solids, which is reported to give improved description of equilibrium properties of solids.[97] The PBE and PBEsol functionals generally underestimate the band gap, which is often addressed by using a hybrid density functional such as HSE06 of Heyd, Scuseria, and Ernzerhof.[98,99] There exists an ambiguity about the role of dispersive interactions in determining structural properties of organic−inorganic halide perovskites. Some of the theoretical studies have shown that it is important to consider dispersive interactions for providing reliable predictions of structural parameters of hybrid halide perovskites.[37,100,101] Bokdam et al. suggested van der Waals (vdW) dispersion interactions did not improve the description of the material, while hybrid functionals and the strongly constrained appropriately normed (SCAN) density functional gave better results.[102] However, the SCAN functional has been suggested to already include some degree of short range dispersion, making its results good.[103] Hence, we have considered DFT methods with and without D3 corrections and examined the geometric and electronic structures. We have included van der Waals dispersion interactions by employing the zero damping DFT-D3 method of Grimme to account for the dispersion interactions.[77] Thus, we have employed PBE, PBEsol, HSE06, PBE+D3, PBEsol+D3, and HSE06+D3 functionals to study the structure and properties of $CH_3NH_3GeI_3$. Geometry optimizations were performed with force convergence criteria as 0.01 eV/Å, over a range of constrained volumes, and the equilibrium cell volume was found by fitting the energy−volume curve to the Murnaghan equation of state,[104] which minimizes the error associated with the Pulay stress.[105] Spin−orbit coupling effects were not considered here as they have been shown to be negligible in germanium-based hybrid perovskites.[58,59] The Brillouin zone and the high symmetry points used to generate band structures are taken from the handbook of Bradley and Cracknell.[106] The optical absorption spectrum was computed by using the transversal approximation and PAW method, which sums the absorption spectra over all direct valence band (VB)-to-conduction band (CB) transitions and therefore ignores indirect and intraband absorption, which, despite ignoring excitonic effects, has given reasonable optical absorption spectra[70,93−98] and revealed if transitions are symmetry-allowed.[79,107−112] We have performed quasiparticle *GW* calculations by carrying out single-shot G_0W_0, partially self-consistent GW_0, and the self-consistent *GW*.[86,113−115] For all *GW* calculations, we employed a plane wave cutoff of 500 eV, 512 bands (20 occupied + 492 unoccupied bands), 8 × 8 × 8 γ-centered *k* point grid, comprising 128 irreducible points. Convergence tests were

DOI: 10.1021/acsomega.8b03291
ACS Omega 2019, 4, 5661−5669

performed from 400 to 1000 bands with convergence at 512 bands of absolute energies of 0.1 eV with the band gap within 0.03 eV. *GW* band structures were calculated by interpolating the wavefunction using Wannier analysis as implemented in the Wannier90 code.[118]

■ ASSOCIATED CONTENT

Supporting Information

The Supporting Information is available free of charge on the ACS Publications website at DOI: 10.1021/acsomega.8b03291.

Band structure and density of states of $CH_3NH_3GeI_3$ obtained using all the methods considered in this study (PDF)

■ AUTHOR INFORMATION

Corresponding Authors

*Email: deivasiu@tcd.ie. Phone: +353 1 896 8488 (D.U.).
*Email: watsong@tcd.ie. Phone: +353 1 896 1357 (G.W.W.).

ORCID

Deivasigamani Umadevi: 0000-0001-9732-2556
Graeme W. Watson: 0000-0001-6732-9474

Notes

The authors declare no competing financial interest.

■ ACKNOWLEDGMENTS

D.U. is grateful to the Irish Research Council postdoctoral fellowship GOIPD/2015/290. This work was supported by the Science Foundation Ireland through the Principal Investigator Programme (grant number 12/IA/1414). Calculations were performed on the Lonsdale cluster, funded through the Science Foundation Ireland, the Kelvin cluster, funded through the Higher Education Authority, through its PRTLI program, both maintained by the Trinity Centre for High Performance Computing, and on the DJEI/DES/SFI/HEA Irish Centre for High-End Computing (ICHEC) platform Fionn.

■ REFERENCES

(1) Peter, L. M. Towards sustainable photovoltaics: The search for new materials. *Philos. Trans. Trans. R. Soc., A* **2011**, *369*, 1840.
(2) Battaglia, C.; Cuevas, A.; De Wolf, S. High-efficiency crystalline silicon solar cells: status and perspectives. *Energy Environ. Sci.* **2016**, *9*, 1552−1576.
(3) Ben Rabha, M.; Mohamed, S. B.; Dimassi, W.; Gaidi, M.; Ezzaouia, H.; Bessais, B. Reduction of absorption loss in multicrystalline silicon via combination of mechanical grooving and porous silicon. *Phys. Status Solidi C* **2011**, *8*, 883−886.
(4) Kazim, S.; Nazeeruddin, M. K.; Grätzel, M.; Ahmad, S. Perovskite as light harvester: A game changer in photovoltaics. *Angew. Chem. Int. Ed.* **2014**, *53*, 2812−2824.
(5) Grätzel, M. The light and shade of perovskite solar cells. *Nat. Mater.* **2014**, *13*, 838−842.
(6) Kojima, A.; Teshima, K.; Shirai, Y.; Miyasaka, T. Organometal halide perovskites as visible-light sensitizers for photovoltaic cells. *J. Am. Chem. Soc.* **2009**, *131*, 6050−6051.
(7) Yang, W. S.; Noh, J. H.; Jeon, N. J.; Kim, Y. C.; Ryu, S.; Seo, J.; Seok, S. I. High-performance photovoltaic perovskite layers fabricated through intramolecular exchange. *Science* **2015**, *348*, 1234−1237.
(8) National Revewable Energy Laboratory. *NREL solar cell efficiency chart*. NREL https://www.nrel.gov/pv/assets/pdfs/pv-efficiency-chart.20190103.pdf. 2019.
(9) Dong, Q.; Fang, Y.; Shao, Y.; Mulligan, P.; Qiu, J.; Cao, L.; Huang, J. Electron-hole diffusion lengths > 175 μm in solution-grown $CH_3NH_3PbI_3$ single crystals. *Science* **2015**, *347*, 967−970.
(10) Zhang, Q.; Ha, S. T.; Liu, X.; Sum, T. C.; Xiong, Q. Room-temperature near-infrared high-Q perovskite whispering-gallery planar nanolasers. *Nano Lett.* **2014**, *14*, 5995−6001.
(11) Fan, J.; Jia, B.; Gu, M. Perovskite-based low-cost and high-efficiency hybrid halide solar cells. *Photonics Res.* **2014**, *2*, 111−120.
(12) Long, R.; Liu, J.; Prezhdo, O. V. Unravelling the effects of grain boundary and chemical doping on electron-hole recombination in $CH_3NH_3PbI_3$ perovskite by time-domain atomistic simulation. *J. Am. Chem. Soc.* **2016**, 3884.
(13) Even, J.; Pedesseau, L.; Katan, C.; Kepenekian, M.; Lauret, J.-S.; Sapori, D.; Deleporte, E. Solid-State Physics Perspective on Hybrid Perovskite Semiconductors. *J. Phys. Chem. C* **2015**, *119*, 10161−10177.
(14) Lee, J.-H.; Deng, Z.; Bristowe, N. C.; Bristowe, P. D.; Cheetham, A. K. The competition between mechanical stability and charge carrier mobility in MA-based hybrid perovskites: insight from DFT. *J. Mater. Chem. C* **2018**, *6*, 12252−12259.
(15) Even, J.; Pedesseau, L.; Dupertuis, M.-A.; Jancu, J.-M.; Katan, C. Electronic model for self-assembled hybrid organic/perovskite semiconductors: Reverse band edge electronic states ordering and spin-orbit coupling. *Phys. Rev. B* **2012**, *86*, 205301.
(16) Even, J.; Pedesseau, L.; Jancu, J.-M.; Katan, C. Importance of Spin−Orbit Coupling in Hybrid Organic/Inorganic Perovskites for Photovoltaic Applications. *J. Phys. Chem. Lett.* **2013**, *4*, 2999−3005.
(17) Even, J.; Pedesseau, L.; Katan, C. Analysis of Multivalley and Multibandgap Absorption and Enhancement of Free Carriers Related to Exciton Screening in Hybrid Perovskites. *J. Phys. Chem. C* **2014**, *118*, 11566−11572.
(18) Neukirch, A. J.; Abate, I. I.; Zhou, L.; Nie, W.; Tsai, H.; Pedesseau, L.; Even, J.; Crochet, J. J.; Mohite, A. D.; Katan, C.; Tretiak, S. Geometry Distortion and Small Polaron Binding Energy Changes with Ionic Substitution in Halide Perovskites. *J. Phys. Chem. Lett.* **2018**, *9*, 7130−7136.
(19) Brivio, F.; Walker, A. B.; Walsh, A. Structural and electronic properties of hybrid perovskites for high-efficiency thin-film photovoltaics from first-principles. *APL Mater.* **2013**, *1*, No. 042111.
(20) Frost, J. M.; Butler, K. T.; Brivio, F.; Hendon, C. H.; van Schilfgaarde, M.; Walsh, A. Atomistic origins of high-performance in hybrid halide perovskite solar cells. *Nano Lett.* **2014**, *14*, 2584−2590.
(21) Frost, J. M.; Butler, K. T.; Walsh, A. Molecular ferroelectric contributions to anomalous hysteresis in hybrid perovskite solar cells. *APL Mater.* **2014**, *2*, No. 081506.
(22) Butler, K. T.; Frost, J. M.; Walsh, A. Ferroelectric materials for solar energy conversion: photoferroics revisited. *Energy Environ. Sci.* **2015**, *8*, 838−848.
(23) Frost, J. M.; Walsh, A. What is moving in hybrid halide perovskite solar cells? *Acc. Chem. Res.* **2016**, *49*, 528−535.
(24) Hendon, C. H.; Yang, R. X.; Burton, L. A.; Walsh, A. Assessment of polyanion (BF_4^- and PF_6^-) substitutions in hybrid halide perovskites. *J. Mater. Chem. A* **2015**, *3*, 9067−9070.
(25) Butler, K. T.; Frost, J. M.; Walsh, A. Band alignment of the hybrid halide perovskites $CH_3NH_3PbCl_3$, $CH_3NH_3PbBr_3$ and $CH_3NH_3PbI_3$. *Mater. Horiz.* **2015**, *2*, 228−231.
(26) Whalley, L. D.; Crespo-Otero, R.; Walsh, A. H-center and V-center defects in hybrid halide perovskites. *ACS Energy Lett.* **2017**, *2*, 2713−2714.
(27) Walsh, A.; Scanlon, D. O.; Chen, S.; Gong, X. G.; Wei, S.-H. Self-regulation mechanism for charged point defects in hybrid halide perovskites. *Angew. Chem. Int. Ed.* **2015**, *54*, 1791−1794.
(28) Walsh, A. Principles of chemical bonding and band gap engineering in hybrid organic−inorganic halide perovskites. *J. Phys. Chem. C* **2015**, *119*, 5755−5760.
(29) Whalley, L. D.; Skelton, J. M.; Frost, J. M.; Walsh, A. Phonon anharmonicity, lifetimes, and thermal transport in $CH_3NH_3PbI_3$ from many-body perturbation theory. *Phys. Rev. B* **2016**, *94*, 220301.
(30) Whalley, L. D.; Frost, J. M.; Jung, Y.-K.; Walsh, A. Perspective: Theory and simulation of hybrid halide perovskites. *J. Chem. Phys.* **2017**, *146*, 220901.

DOI: 10.1021/acsomega.8b03291
ACS Omega 2019, 4, 5661−5669

(31) Mosconi, E.; Etienne, T.; De Angelis, F. Rashba band splitting in organohalide lead perovskites: Bulk and surface effects. *J. Phys. Chem. Lett.* **2017**, *8*, 2247−2252.
(32) Quarti, C.; Mosconi, E.; Ball, J. M.; D'Innocenzo, V.; Tao, C.; Pathak, S.; Snaith, H. J.; Petrozza, A.; De Angelis, F. Structural and optical properties of methylammonium lead iodide across the tetragonal to cubic phase transition: implications for perovskite solar cells. *Energy Environ. Sci.* **2016**, *9*, 155−163.
(33) De Angelis, F. Modeling materials and processes in hybrid/organic photovoltaics: From dye-sensitized to perovskite solar cells. *Acc. Chem. Res.* **2014**, *47*, 3349−3360.
(34) Mosconi, E.; Amat, A.; Nazeeruddin, M. K.; Grätzel, M.; De Angelis, F. First-principles modeling of mixed halide organometal perovskites for photovoltaic applications. *J. Phys. Chem. C* **2013**, *117*, 13902−13913.
(35) Umari, P.; Mosconi, E.; De Angelis, F. Infrared dielectric screening determines the low exciton binding energy of metal-halide perovskites. *J. Phys. Chem. Lett.* **2018**, *9*, 620−627.
(36) Amat, A.; Mosconi, E.; Ronca, E.; Quarti, C.; Umari, P.; Nazeeruddin, M. K.; Grätzel, M.; De Angelis, F. Cation-induced band-gap tuning in organohalide perovskites: Interplay of spin−orbit coupling and octahedra tilting. *Nano Lett.* **2014**, *14*, 3608−3616.
(37) Motta, C.; El-Mellouhi, F.; Kais, S.; Tabet, N.; Alharbi, F.; Sanvito, S. Revealing the role of organic cations in hybrid halide perovskite $CH_3NH_3PbI_3$. *Nat. Commun.* **2015**, *6*, 7026.
(38) Aristidou, N.; Sanchez-Molina, I.; Chotchuangchutchaval, T.; Brown, M.; Martinez, L.; Rath, T.; Haque, S. A. The role of oxygen in the degradation of methylammonium lead trihalide perovskite photoactive layers. *Angew. Chem. Int. Ed.* **2015**, *54*, 8208−8212.
(39) Li, X.; Dar, M. I.; Yi, C.; Luo, J.; Tschumi, M.; Zakeeruddin, S. M.; Nazeeruddin, M. K.; Han, H.; Grätzel, M. Improved performance and stability of perovskite solar cells by crystal crosslinking with alkylphosphonic acid ω-ammonium chlorides. *Nat. Chem.* **2015**, *7*, 703−711.
(40) Smith, I. C.; Hoke, E. T.; Solis-Ibarra, D.; McGehee, M. D.; Karunadasa, H. I. A layered hybrid perovskite solar-cell absorber with enhanced moisture stability. *Angew. Chem. Int. Ed.* **2014**, *53*, 11232−11235.
(41) McMeekin, D. P.; Sadoughi, G.; Rehman, W.; Eperon, G. E.; Saliba, M.; Hörantner, M. T.; Haghighirad, A.; Sakai, N.; Korte, L.; Rech, B.; Johnston, M. B.; Herz, L. M.; Snaith, H. J. A mixed-cation lead mixed-halide perovskite absorber for tandem solar cells. *Science* **2016**, *351*, 151.
(42) Beal, R. E.; Slotcavage, D. J.; Leijtens, T.; Bowring, A. R.; Belisle, R. A.; Nguyen, W. H.; Burkhard, G. F.; Hoke, E. T.; McGehee, M. D. Cesium lead halide perovskites with improved stability for tandem solar cells. *J. Phys. Chem. Lett.* **2016**, *7*, 746−751.
(43) Ganose, A. M.; Butler, K. T.; Walsh, A.; Scanlon, D. O. Relativistic electronic structure and band alignment of BiSI and BiSeI: candidate photovoltaic materials. *J. Mater. Chem. A* **2016**, *4*, 2060−2068.
(44) Savory, C. N.; Walsh, A.; Scanlon, D. O. Can Pb-free halide double perovskites support high-efficiency solar cells? *ACS Energy Lett.* **2016**, *1*, 949−955.
(45) Ganose, A. M.; Savory, C. N.; Scanlon, D. O. Beyond methylammonium lead iodide: Prospects for the emergent field of ns^2 containing solar absorbers. *Chem. Commun.* **2017**, *53*, 20−44.
(46) Savory, C. N.; Ganose, A. M.; Scanlon, D. O. Exploring the $PbS-Bi_2S_3$ series for next generation energy conversion materials. *Chem. Mater.* **2017**, *29*, 5156−5167.
(47) Savory, C. N.; Palgrave, R. G.; Bronstein, H.; Scanlon, D. O. Spatial electron-hole separation in a one dimensional hybrid organic−inorganic lead iodide. *Sci. Rep.* **2016**, *6*, 20626.
(48) Wang, Z.; Ganose, A. M.; Niu, C.; Scanlon, D. O. First-principles insights into tin-based two-dimensional hybrid halide perovskites for photovoltaics. *J. Mater. Chem. A* **2018**, *6*, 5652−5660.
(49) Ganose, A. M.; Savory, C. N.; Scanlon, D. O. Electronic and defect properties of $(CH_3NH_3)_2Pb(SCN)_2I_2$ analogues for photovoltaic applications. *J. Mater. Chem. A* **2017**, *5*, 7845−7853.
(50) Ganose, A. M.; Savory, C. N.; Scanlon, D. O. $(CH_3NH_3)_2Pb(SCN)_2I_2$: A more stable structural motif for hybrid halide photovoltaics? *J. Phys. Chem. Lett.* **2015**, *6*, 4594−4598.
(51) Hao, F.; Stoumpos, C. C.; Chang, R. P. H.; Kanatzidis, M. G. Anomalous band gap behavior in mixed Sn and Pb perovskites enables broadening of absorption spectrum in solar cells. *J. Am. Chem. Soc.* **2014**, *136*, 8094−8099.
(52) Bernal, C.; Yang, K. First-principles hybrid functional study of the organic−inorganic perovskites $CH_3NH_3SnBr_3$ and $CH_3NH_3SnI_3$. *J. Phys. Chem. C* **2014**, *118*, 24383−24388.
(53) Hao, F.; Stoumpos, C. C.; Cao, D. H.; Chang, R. P. H.; Kanatzidis, M. G. Lead-free solid-state organic-inorganic halide perovskite solar cells. *Nat. Photonics* **2014**, *8*, 489−494.
(54) Noel, N. K.; Stranks, S. D.; Abate, A.; Wehrenfennig, C.; Guarnera, S.; Haghighirad, A.-A.; Sadhanala, A.; Eperon, G. E.; Pathak, S. K.; Johnston, M. B.; Petrozza, A.; Herz, L. M.; Snaith, H. J. Lead-free organic-inorganic tin halide perovskites for photovoltaic applications. *Energy Environ. Sci.* **2014**, *7*, 3061−3068.
(55) McClure, E. T.; Ball, M. R.; Windl, W.; Woodward, P. M. Cs_2AgBiX_6 (X = Br, Cl): New visible light absorbing, lead-free halide perovskite semiconductors. *Chem. Mater.* **2016**, *28*, 1348−1354.
(56) Filip, M. R.; Hillman, S.; Haghighirad, A. A.; Snaith, H. J.; Giustino, F. Band gaps of the lead-free halide double perovskites $Cs_2BiAgCl_6$ and $Cs_2BiAgBr_6$ from theory and experiment. *J. Phys. Chem. Lett.* **2016**, *7*, 2579−2585.
(57) Zhao, X.-G.; Yang, J.-H.; Fu, Y.; Yang, D.; Xu, Q.; Yu, L.; Wei, S.-H.; Zhang, L. Design of lead-free inorganic halide perovskites for solar cells via cation-transmutation. *J. Am. Chem. Soc.* **2017**, *139*, 2630−2638.
(58) Zhao, Y.-Q.; Liu, B.; Yu, Z.-L.; Ma, J.; Wan, Q.; He, P.-b.; Cai, M.-Q. Strong ferroelectric polarization of $CH_3NH_3GeI_3$ with high-absorption and mobility transport anisotropy: theoretical study. *J. Mater. Chem. C* **2017**, *5*, 5356−5364.
(59) Lu, X.; Zhao, Z.; Li, K.; Han, Z.; Wei, S.; Guo, C.; Zhou, S.; Wu, Z.; Guo, W.; Wu, C. M. L. First-principles insight into the photoelectronic properties of Ge-based perovskites. *RSC Adv.* **2016**, *6*, 86976−86981.
(60) Zhao, Y.-Q.; Wang, X.; Liu, B.; Yu, Z.-L.; He, P.-B.; Wan, Q.; Cai, M.-Q.; Yu, H.-L. Geometric structure and photovoltaic properties of mixed halide germanium perovskites from theoretical view. *Org. Electron.* **2018**, *53*, 50−56.
(61) Stoumpos, C. C.; Frazer, L.; Clark, D. J.; Kim, Y. S.; Rhim, S. H.; Freeman, A. J.; Ketterson, J. B.; Jang, J. I.; Kanatzidis, M. G. Hybrid germanium iodide perovskite semiconductors: Active lone pairs, structural distortions, direct and indirect energy gaps, and strong nonlinear optical properties. *J. Am. Chem. Soc.* **2015**, *137*, 6804−6819.
(62) Krishnamoorthy, T.; Ding, H.; Yan, C.; Leong, W. L.; Baikie, T.; Zhang, Z.; Sherburne, M.; Li, S.; Asta, M.; Mathews, N.; Mhaisalkar, S. G. Lead-free germanium iodide perovskite materials for photovoltaic applications. *J. Mater. Chem. A* **2015**, *3*, 23829−23832.
(63) Sun, P.-P.; Li, Q.-S.; Yang, L.-N.; Li, Z.-S. Theoretical insights into a potential lead-free hybrid perovskite: substituting Pb^{2+} with Ge^{2+}. *Nanoscale* **2016**, *8*, 1503−1512.
(64) Zhao, Y.-Q.; Liu, B.; Yu, Z.-L.; Cao, D.; Cai, M.-Q. Tuning charge carrier types, superior mobility and absorption in lead-free perovskite $CH_3NH_3GeI_3$: Theoretical study. *Electrochim. Acta* **2017**, *247*, 891−898.
(65) Lee, J.-H.; Bristowe, N. C.; Bristowe, P. D.; Cheetham, A. K. Role of hydrogen-bonding and its interplay with octahedral tilting in CH3NH3PbI3. *Chem. Commun.* **2015**, *51*, 6434−6437.
(66) Lee, J.-H.; Bristowe, N. C.; Lee, J. H.; Lee, S.-H.; Bristowe, P. D.; Cheetham, A. K.; Jang, H. M. Resolving the Physical Origin of Octahedral Tilting in Halide Perovskites. *Chem. Mater.* **2016**, *28*, 4259−4266.
(67) Giorgi, G.; Fujisawa, J.-I.; Segawa, H.; Yamashita, K. Small photocarrier effective masses featuring ambipolar transport in methylammonium lead iodide perovskite: A density functional analysis. *J. Phys. Chem. Lett.* **2013**, *4*, 4213−4216.

DOI: 10.1021/acsomega.8b03291
ACS Omega 2019, 4, 5661−5669

(68) Allen, F. H.; Kennard, O.; Watson, D. G.; Brammer, L.; Orpen, A. G.; Taylor, R. Tables of bond lengths determined by X-ray and neutron diffraction. Part 1. Bond lengths in organic compounds. *J. Chem. Soc., Perkin Trans. 2* **1987**, *0*, S1−S19.
(69) Menéndez-Proupin, E.; Palacios, P.; Wahnón, P.; Conesa, J. C. Self-consistent relativistic band structure of the $CH_3NH_3PbI_3$ perovskite. *Phys. Rev. B* **2014**, *90*, No. 045207.
(70) Giorgi, G.; Fujisawa, J.-I.; Segawa, H.; Yamashita, K. Cation Role in Structural and Electronic Properties of 3D Organic−Inorganic Halide Perovskites: A DFT Analysis. *J. Phys. Chem. C* **2014**, *118*, 12176−12183.
(71) Eames, C.; Frost, J. M.; Barnes, P. R. F.; O'Regan, B. C.; Walsh, A.; Islam, M. S. Ionic transport in hybrid lead iodide perovskite solar cells. *Nat. Commun.* **2015**, *6*, 7497.
(72) Baikie, T.; Fang, Y.; Kadro, J. M.; Schreyer, M.; Wei, F.; Mhaisalkar, S. G.; Graetzel, M.; White, T. J. Synthesis and crystal chemistry of the hybrid perovskite $(CH_3NH_3)PbI_3$ for solid-state sensitised solar cell applications. *J. Mater. Chem. A* **2013**, *1*, 5628−5641.
(73) Weller, M. T.; Weber, O. J.; Henry, P. F.; Di Pumpo, A. M.; Hansen, T. C. Complete structure and cation orientation in the perovskite photovoltaic methylammonium lead iodide between 100 and 352 K. *Chem. Commun.* **2015**, *51*, 4180−4183.
(74) Govinda, S.; Mahale, P.; Kore, B. P.; Mukherjee, S.; Pavan, M. S.; De, C.; Ghara, S.; Sundaresan, A.; Pandey, A.; Guru Row, T. N.; Sarma, D. D. Is $CH_3NH_3PbI_3$ Polar? *J. Phys. Chem. Lett.* **2016**, *7*, 2412−2419.
(75) Dang, Y.; Liu, Y.; Sun, Y.; Yuan, D.; Liu, X.; Lu, W.; Liu, G.; Xia, H.; Tao, X. Bulk crystal growth of hybrid perovskite material CH3NH3PbI3. *CrystEngComm* **2015**, *17*, 665−670.
(76) Stoumpos, C. C.; Malliakas, C. D.; Kanatzidis, M. G. Semiconducting Tin and Lead Iodide Perovskites with Organic Cations: Phase Transitions, High Mobilities, and Near-Infrared Photoluminescent Properties. *Inorg. Chem.* **2013**, *52*, 9019−9038.
(77) Grimme, S.; Antony, J.; Ehrlich, S.; Krieg, H. A consistent and accurate ab initio parametrization of density functional dispersion correction (DFT-D) for the 94 elements H-Pu. *J. Chem. Phys.* **2010**, *132*, 154104.
(78) Tanaka, K.; Takahashi, T.; Ban, T.; Kondo, T.; Uchida, K.; Miura, N. Comparative study on the excitons in lead-halide-based perovskite-type crystals $CH_3NH_3PbBr_3$ $CH_3NH_3PbI_3$. *Solid State Commun.* **2003**, *127*, 619−623.
(79) Gajdoš, M.; Hummer, K.; Kresse, G.; Furthmüller, J.; Bechstedt, F. Linear optical properties in the projector-augmented wave methodology. *Phys. Rev. B* **2006**, *73*, No. 045112.
(80) Bokdam, M.; Sander, T.; Stroppa, A.; Picozzi, S.; Sarma, D. D.; Franchini, C.; Kresse, G. Role of polar phonons in the photo excited state of metal halide perovskites. *Sci. Rep.* **2016**, *6*, 28618.
(81) Brivio, F.; Butler, K. T.; Walsh, A.; van Schilfgaarde, M. Relativistic quasiparticle self-consistent electronic structure of hybrid halide perovskite photovoltaic absorbers. *Phys. Rev. B* **2014**, *89*, 155204.
(82) Umari, P.; Mosconi, E.; De Angelis, F. Relativistic GW calculations on $CH_3NH_3PbI_3$ and $CH_3NH_3SnI_3$ Perovskites for Solar Cell Applications. *Sci. Rep.* **2014**, *4*, 4467.
(83) Filip, M. R.; Verdi, C.; Giustino, F. GW band structures and carrier effective masses of $CH_3NH_3PbI_3$ and hypothetical perovskites of the type $APbI_3$: A = NH_4, PH_4, AsH_4, and SbH_4. *J. Phys. Chem. C* **2015**, *119*, 25209−25219.
(84) Gao, W.; Gao, X.; Abtew, T. A.; Sun, Y.-Y.; Zhang, S.; Zhang, P. Quasiparticle band gap of organic-inorganic hybrid perovskites: Crystal structure, spin-orbit coupling, and self-energy effects. *Phys. Rev. B* **2016**, *93*, No. 085202.
(85) Wiktor, J.; Rothlisberger, U.; Pasquarello, A. Predictive Determination of Band Gaps of Inorganic Halide Perovskites. *J. Phys. Chem. Lett.* **2017**, *8*, 5507−5512.
(86) Bruneval, F.; Vast, N.; Reining, L. Effect of self-consistency on quasiparticles in solids. *Phys. Rev. B* **2006**, *74*, No. 045102.
(87) Holm, B.; von Barth, U. Fully self-consistent *GW* self-energy of the electron gas. *Phys. Rev. B* **1998**, *57*, 2108−2117.
(88) Tamme, D.; Schepe, R.; Henneberger, K. Comment on "Self-Consistent Calculations of Quasiparticle States in Metals and Semiconductors". *Phys. Rev. Lett.* **1999**, *83*, 241−241.
(89) van Schilfgaarde, M.; Kotani, T.; Faleev, S. Quasiparticle Self-Consistent *GW* Theory. *Phys. Rev. Lett.* **2006**, *96*, 226402.
(90) Madelung, O. *Semiconductors: Data Handbook*; Springer-Verlag: Berlin Heidelberg, 2004.
(91) Shockley, W.; Queisser, H. J. Detailed balance limit of efficiency of *p-n* junction solar cells. *J. Appl. Phys.* **1961**, *32*, 510−519.
(92) Kresse, G.; Hafner, J. *Ab initio* molecular-dynamics simulation of the liquid-metal-amorphous-semiconductor transition in germanium. *Phys. Rev. B* **1994**, *49*, 14251−14269.
(93) Kresse, G.; Furthmüller, J. Efficiency of ab-initio total energy calculations for metals and semiconductors using a plane-wave basis set. *Comput. Mater. Sci.* **1996**, *6*, 15−50.
(94) Blöchl, P. E. Projector augmented-wave method. *Phys. Rev. B* **1994**, *50*, 17953−17979.
(95) Kresse, G.; Joubert, D. From ultrasoft pseudopotentials to the projector augmented-wave method. *Phys. Rev. B* **1999**, *59*, 1758−1775.
(96) Perdew, J. P.; Burke, K.; Ernzerhof, M. Generalized gradient approximation made simple. *Phys. Rev. Lett.* **1996**, *77*, 3865−3868.
(97) Perdew, J. P.; Ruzsinszky, A.; Csonka, G. I.; Vydrov, O. A.; Scuseria, G. E.; Constantin, L. A.; Zhou, X.; Burke, K. Restoring the density-gradient expansion for exchange in solids and surfaces. *Phys. Rev. Lett.* **2008**, *100*, 136406.
(98) Heyd, J.; Scuseria, G. E.; Ernzerhof, M. Hybrid functionals based on a screened Coulomb potential. *J. Chem. Phys.* **2003**, *118*, 8207−8215.
(99) Heyd, J.; Scuseria, G. E.; Ernzerhof, M. Erratum: "Hybrid functionals based on a screened Coulomb potential" [J. Chem. Phys. 118, 8207 (2003)]. *J. Chem. Phys.* **2006**, *124*, 219906.
(100) Egger, D. A.; Kronik, L. Role of dispersive interactions in determining structural properties of organic−inorganic halide perovskites: Insights from first-principles calculations. *J. Phys. Chem. Lett.* **2014**, *5*, 2728−2733.
(101) Geng, W.; Zhang, L.; Zhang, Y.-N.; Lau, W.-M.; Liu, L.-M. First-principles study of lead iodide perovskite tetragonal and orthorhombic phases for photovoltaics. *J. Phys. Chem. C* **2014**, *118*, 19565−19571.
(102) Bokdam, M.; Lahnsteiner, J.; Ramberger, B.; Schäfer, T.; Kresse, G. Assessing Density Functionals Using Many Body Theory for Hybrid Perovskites. *Phys. Rev. Lett.* **2017**, *119*, 145501.
(103) Brandenburg, J. G.; Bates, J. E.; Sun, J.; Perdew, J. P. Benchmark tests of a strongly constrained semilocal functional with a long-range dispersion correction. *Phys. Rev. B* **2016**, *94*, 115144.
(104) Murnaghan, F. D. The compressibility of media under extreme pressures. *Proc. Natl. Acad. Sci. U. S. A.* **1944**, *30*, 244−247.
(105) Allen, J. P.; Scanlon, D. O.; Parker, S. C.; Watson, G. W. Tin monoxide: Structural prediction from first principles calculations with van der waals corrections. *J. Phys. Chem. C* **2011**, *115*, 19916−19924.
(106) Bradley, C. J.; Cracknell, A. P. *Mathematical theory of symmetry in solids*; Oxford University Press, 1972.
(107) Allen, J. P.; Scanlon, D. O.; Watson, G. W. Electronic structures of silver oxides. *Phys. Rev. B* **2011**, *84*, 115141.
(108) Godinho, K. G.; Carey, J. J.; Morgan, B. J.; Scanlon, D. O.; Watson, G. W. Understanding conductivity in $SrCu_2O_2$: stability, geometry and electronic structure of intrinsic defects from first principles. *J. Mater. Chem.* **2010**, *20*, 1086−1096.
(109) Kehoe, A. B.; Temple, D. J.; Watson, G. W.; Scanlon, D. O. Cu_3MCh_3 (M = Sb, Bi; Ch = S, Se) as candidate solar cell absorbers: insights from theory. *Phys. Chem. Chem. Phys.* **2013**, *15*, 15477−15484.
(110) Scanlon, D. O.; Walsh, A.; Watson, G. W. Understanding the p-type conduction properties of the transparent conducting oxide $CuBO_2$: A density functional theory analysis. *Chem. Mater.* **2009**, *21*, 4568−4576.

DOI: 10.1021/acsomega.8b03291
ACS Omega 2019, 4, 5661−5669

(111) Scanlon, D. O.; Watson, G. W. $(Cu_2S_2)(Sr_3Sc_2O_5)^{-}$a layered, direct band gap, p-type transparent conducting oxychalcogenide: A theoretical analysis. *Chem. Mater.* **2009**, *21*, 5435−5442.
(112) Nie, X.; Wei, S.-H.; Zhang, S. B. Bipolar doping and band-gap anomalies in delafossite transparent conductive oxides. *Phys. Rev. Lett.* **2002**, *88*, No. 066405.
(113) Shishkin, M.; Marsman, M.; Kresse, G. Accurate quasiparticle spectra from self-consistent *GW* calculations with vertex corrections. *Phys. Rev. Lett.* **2007**, *99*, 246403.
(114) Hedin, L. New method for calculating the one-particle green's function with application to the electron-gas problem. *Phys. Rev.* **1965**, *139*, A796−A823.
(115) Shishkin, M.; Kresse, G. Implementation and performance of the frequency-dependent *GW* method within the PAW framework. *Phys. Rev. B* **2006**, *74*, No. 035101.
(116) Mostofi, A. A.; Yates, J. R.; Lee, Y.-S.; Souza, I.; Vanderbilt, D.; Marzari, N. Wannier90: A tool for obtaining maximally-localised Wannier functions. *Comput. Phys. Commun.* **2008**, *178*, 685−699.

DOI: 10.1021/acsomega.8b03291
ACS Omega 2019, 4, 5661−5669